0026-895X/06/6905-1673–1683$20.00
MOLECULAR PHARMACOLOGY
Vol. 69, No. 5
19729/3113140
Mol Pharmacol 69:1673–1683, 2006
Printed in U.S.A.

Species Diversity and Peptide Toxins Blocking Selectivity of *Ether-à-go-go*–Related Gene Subfamily K^+ Channels in the Central Nervous System

Rita Restano-Cassulini, Yuliya V. Korolkova, Sylvie Diochot, Georgina Gurrola, Leonardo Guasti, Lourival D. Possani, Michel Lazdunski, Eugene V. Grishin, Annarosa Arcangeli, and Enzo Wanke

Dipartimento di Biotecnologie e Bioscienze, Università di Milano-Bicocca, Milano, Italy (R.R.-C., E.W.); Shemyakin-Ovchinnikov Intitute of Bioorganic Chemistry, Russian Academy of Sciences, Moscow, Russia (Y.V.K., E.V.G.); Institut de Pharmacologie Moléculaire et Cellulaire, Centre National de la Recherche Scientifique-Unité Mixte Recherche, Valbonne, France (S.D., M.L.); Department of Molecular Medicine and Bioprocesses, Institute of Biotechnology, National Autonomous University of Mexico, Cuernavaca, Mexico (G.G., L.D.P.); and Dipartimento di Patologia e Oncologia Sperimentali, Università di Firenze, Firenze, Italy (L.G., A.A.)

Received October 10, 2005; accepted February 23, 2006

ABSTRACT

The *ether-à-go-go*-related gene (erg) K^+ channels are known to be crucial for life in *Caenorhabditis elegans* (mating), *Drosophila melanogaster* (seizure), and humans (LQT syndrome). The *erg* genes known to date (*erg1*, *erg2*, and *erg3*) are highly expressed in various areas of the rat and mouse central nervous system (CNS), and ERG channel blockers alter firing accommodation. To assign physiological roles to each isoform, it is necessary to design pharmacological strategies to distinguish individual currents. To this purpose, we have investigated the blocking properties of specific peptide inhibitors of hERG1 channels on the human and rat isoforms. In particular, we have tested ErgTx1 (from the scorpion *Centruroides noxious*), BeKm-1 (from the scorpion *Buthus eupeus*), and APETx1 (from the sea anemone *Anthopleura elegantissima*). Because these peptides had different species-specific effects on the six different channels, we have also carried out a biophysical characterization of hERG2 and hERG3 channels that turned out to be different from the rat homologs. It emerged that APETx1 is exquisitely selective for ERG1 and does not compete with the other two toxins. BeKm-1 discriminates well among the three rat members. ErgTx1 is unable to block hERG2, but blocks rERG2 and has the lowest K_D for hERG3. BeKm-1 and ErgTx1 compete for hERG3 but not for rERG2 blockade. Our findings should be helpful for structure-function studies and for novel CNS ERG-specific drug design.

The *ether-à-go-go* family of voltage-dependent K^+ channels consists of the *eag*, *elk* (*eag*-like), and *erg* (*eag*-related gene) subfamilies (Warmke and Ganetzky, 1994). The ERG subfamily comprises ERG1, ERG2, and ERG3 (Shi et al., 1997), which may form either homo- or heterotetramers (Wimmers et al., 2001, 2002).

hERG1 (Warmke and Ganetzky, 1994; Titus et al., 1997) regulates the duration of the cardiac action potential (Sanguinetti et al., 1995); in fact, the slowly decreasing action potential plateau shifts these channels to a less inactivated state that increases the outward K^+ current, thus sustaining further repolarization (Sanguinetti and Jurkiewicz, 1990). ERG1 channels may also sustain a process of spike-frequency adaptation (Chiesa et al., 1997), thus contributing to control burst duration in smooth muscle (Akbarali et al., 1999), carotid body (Overholt et al., 2000), lactotrophs (Corrette et al., 1996; Lecchi et al., 2002), human pancreatic β cells (Ro-

This study was partially supported by grants from the Italian Ministero dell'Università e della Ricerca Scientifica e Tecnologica (MIUR-PRIN2003-2005-2001055320 and 2003052919, MIUR-FIRB2001-RBNE01XMP4-002, MIUR-FISR2001-0300179), the Università di Milano-Bicocca (to E.W. and to A.A.) (MIUR-PRIN2003-2005-2003054500), and by Telethon Fondazione Onlus (GGP02208 to A.A.). It also was supported by the National Council of Science and Technology (Mexican Government, grant 40251-Q) and from the *Dirección General de Asuntos de Personal Académico* (grant IN206003) of the National Autonomous University of Mexico (to L.D.P.). R.R.-C. is a Ph.D. student of Physiology at the Department of Biotechnologies and Biosciences of the University of Milano-Bicocca. These data were presented in part as a poster at the 2005 Neuroscience Meeting, 152.4.

All laboratories contributed equally to the manuscript.

Article, publication date, and citation information can be found at http://molpharm.aspetjournals.org.

doi:10.1124/mol.105.019729.

ABBREVIATIONS: CNS, central nervous system; ERG, *ether-à-go-go*-related gene; *Erg*, *ether-à-go-go*-related gene; hERG, human *ether-à-go-go*-related gene channel; rERG, rat *ether-à-go-go*-related gene channel; WAY123,398, *N*-methyl-*N*-(2-(methyl(1-methyl-1*H*-benzimidazol-2-yl)amino)ethyl)-4-((methylsulfonyl)amino)benzenesulfonamide; UCF, unblocked channel fraction.

sati et al., 2000), and chromaffin cells (Gullo et al., 2003). It has been shown that all the members of the ERG subfamily are expressed in the CNS in both rat (Saganich et al., 2001; Papa et al., 2003) and mouse (Polvani et al., 2003; Guasti et al., 2005). Evidence of the functional significance of this expression has been obtained in mouse cerebellar Purkinje cells and in rat embryonic rhombencephalon neurons (Sacco et al., 2003; Hirdes et al., 2005).

To decipher the functional role of ERG in CNS, it is necessary to isolate the different contributions given by each member of the subfamily. Organic and peptide blockers are known for hERG1 channels. The HERG organic blockers are not sufficiently selective for the different isoforms. However, several hERG-specific peptides have become available: ErgTx1 (CnErg1; Gurrola et al., 1999), ErgTx2 (Lecchi et al., 2002), BeKm-1 (Korolkova et al., 2001), CsEKerg1 (Nastainczyk et al., 2002), and APETx1 (Diochot et al., 2003). The aim of the present study was to examine whether the above ERG1-specific peptides present selective effects on different ERG members. The rationale for this study was the observation that the amino acid sequence of the extracellular "S5-P linker" pore region is different in the three ERG isoforms (Torres et al., 2003). This segment is the putative binding site for the scorpion toxins.

Our results show that 1) the blocking effect of our peptides was reversible (approximately 1 min), with two exceptions (ErgTx1 on hERG3, and rERG2 and BeKm1 on rERG2); 2) APETx1 turned out to be a selective blocker for ERG1; 3) ErgTx1 was unable to block hERG2; and 4) dose-response curves for ErgTx1 and BeKm-1 overlapped. The above differences prompted us to investigate in more detail the biophysical properties of the human and rat ERG2 and ERG3 channels that turned out to be different.

Materials and Methods

Plasmids

rerg1, rerg2, and rerg3 cDNAs were kindly provided by Prof. J. R. Schwarz (University of Hamburg, Hamburg, Germany). Herg2 and herg3 cDNAs were excised from pGH19 vectors (kindly provided by Prof. B. Ganetzky, University of Wisconsin, Madison, WI) and cloned into pCDNA3.1 vector (Invitrogen, Carlsbad, CA). The hERG2 cDNA received from Prof. B. Ganetzky slightly differs from the sequence deposited at NCBI (accession number NP110406) because it lacks a stretch of nucleotides coding for amino acids 718 to 729.

Toxins

ErgTx1, BeKm-1, and APETx1 were purified in the laboratories of Profs. Possani, Grishin, and Lazdunsky, respectively, as described previously (Gurrola et al., 1999; Korolkova et al., 2001; Diochot et al., 2003).

Electrophysiology

Cell Culture. Chinese hamster ovary cells were routinely cultured in Dulbecco's modified Eagle's medium (Invitrogen, Carlsbad, CA) containing 10% fetal calf serum (Invitrogen) and maintained at 37°C in humidified atmosphere with 5% CO_2. Approximately 2×10^4 cells were transfected with 1 to 5 μg of the appropriate plasmid, along with 0.2 μg of green fluorescent protein coding plasmid (pEGFP-C1; Clontech, Mountain View, CA). For transfection, a Lipofectamine reagent kit (Invitrogen) was used, following the instructions of the manufacturer. Currents were recorded 24 to 72 h after transfection.

Solutions and Drugs. During the patch-clamp experiments cells were maintained in our standard extracellular solution, containing: 130 mM NaCl, 5 mM KCl, 2 mM $CaCl_2$, 2 mM $MgCl_2$, 10 mM HEPES-NaOH, and 5 mM D-glucose, pH 7.40. During the specific biophysical tests, cells were perfused with a high K^+ external solution ($[K^+]_o$ = 40 mM), in which NaCl was replaced by an equimolar amount of KCl. The pipette solution contained 130 mM K^+-aspartate, 10 mM NaCl, 2 mM $MgCl_2$, 10 mM EGTA-KOH, and 10 mM HEPES-KOH, pH 7.30, and nominal $[Ca^{2+}]_i$ of ~50 nM. Appropriate quantities of the toxins from stocks in H_2O were dissolved in the extracellular solution immediately before the experiments. When contaminating potassium currents were present, the specific ERG blocker WAY123,398 (Spinelli et al., 1993) was used at 2 μM and the resulting traces were subtracted from control traces to obtain the WAY123,398-sensitive currents. The extracellular solutions were delivered through a nine-hole (0.6-mm) remote-controlled linear positioner with an average response time of 1 to 2 s that was placed near the cell under study.

Patch-Clamp Recordings and Data Analysis. ERG currents were always elicited under conditions of relatively high $[K]_o$ (40 mM) to measure currents under optimal signal-to-noise conditions. The currents were recorded at room temperature by means of the MultiClamp 700A (Molecular Devices, Sunnyvale, CA), as described previously (Oliveira et al., 2004). Pipette resistances were approximately 1.5 to 2.2 MΩ. Cell capacitance and series resistance errors were compensated (85–90%) before each voltage clamp protocol run to reduce the voltage errors to less than 5% of the protocol pulse. pClamp 8.2 (Molecular Devices) and Origin 7 (OriginLab Corp., Northampton, MA) software were routinely used during data acquisition and analysis.

The steady-state activation curves were obtained by plotting the peak tail currents at −120 mV versus the preconditioning potential (−80 to +30 mV, for 15 s; Fig. 1A), as reported previously (Schönherr et al., 1999). To generate steady-state inactivation curves, we applied the protocol shown in Fig. 1B. In this way, we obtained the currents at each V_m (Fig. 1B, right inset, a and c, ◇). The time to peak of these currents was used to choose the time of the subsequent voltage steps at +20 mV to obtain peak tail currents after different degrees of inactivation (Fig. 1B, right inset, b and c, ——). To compensate for the channel closing at negative potentials, we extrapolated the decaying phase of deactivation to the onset of the test pulse and applied the same relative correction to the peak tail current, as reported previously (Smith et al., 1996). This correction procedure was applied only at the V_m values indicated by asterisks (Fig. 1B, right inset, c, *). The peak tail currents were plotted versus membrane potentials and the curves were best fitted with a Boltzmann function.

Analysis of the Toxin Blockade Data

According to the Clark occupancy model (whose crucial assumption is that response is generated with sufficiently small delay), we assume that the interaction of a blocking toxin and an ion channel is described, at the steady-state, by the classic Michaelis-Menten-type saturating equation (see Gutfreund, 1995). To generate dose-response curves, we have plotted the fraction of unblocked channels (UCF) versus the toxin concentration ([T]). In Clark's model, this corresponds to the probability of receptor vacancy. It should be remembered in fact that

$$K_D = [T](1/UCF - 1)^{-1} \quad (1)$$

Because during long electrophysiological experiments the dose-response curves cannot be obtained under truly steady-state conditions, we preferred to derive the equilibrium dissociation constant K_D from the kinetics of our currents, at different toxin concentrations. Under a typical ON kinetics experiment, if a fixed toxin concentration [T] is applied at time 0, the normalized amplitude of the corresponding outward current, originating from the blockade of a K^+ ion channel, is an exponential decaying function whose time

constant, τ_{on}, is given by $(k_1[T] + k_{-1})^{-1}$, where k_1 and k_{-1} are the association and dissociation rate constants, respectively. On the contrary, in a washout experiment, the exponential increasing function is given by $(1 - \exp(-t/\tau_{off}))$, where τ_{off} is $1/k_{-1}$, which depends only on the dissociation constant k_{-1} and not on [T]. In general,

$$K_D = [T]\tau_{on}/(\tau_{off} - \tau_{on}) \quad (2)$$

By combining eqs. 1 and 2, we obtain.

$$UCF([T]) = \tau_{on}/\tau_{off} \quad (3)$$

The above relation can be used to calculate τ_{off} when it is too long or to estimate τ_{on} when it is too short to be measured for technical reasons.

The time constant of an ON kinetic experiment at concentration [T] at known K_D can be estimated by

$$\tau_{on} = \tau_{off}/(1 + [T]/K_D) \quad (4)$$

which suggests that the experimental perfusing time should be of the order of 4 τ_{on}.

By simple algebraic combination of two ON experiments done at different toxin concentrations, $[T_1]$ and $[T_2]$, which are governed by the time constants τ_{1on} and τ_{2on}, respectively, it results that K_D can be evaluated independently of τ_{off} and is equal to:

$$K_D = ([T_2]\tau_{2on} - [T_1]\tau_{1on})/(\tau_{1on} - \tau_{2on}) \quad (5)$$

which can be easily evaluated by measuring experimentally only the two block time constants and not the washout time constant, as in eq. 2.

Results

The sequences of the S5–S6 linker region of the rat and human ERG channels are shown in Table 1 (the black background indicates the hypothesized α-helix; Zhang et al., 2003). They show that the ERG isoforms present several differences, and there are also differences between human and rat sequences of the same family. According to various cited studies, it is expected that BeKm-1 and ErgTx1 bind to the residues indicated in white. Some of these are targets of both toxins (black background). No similar data are available for APETx1.

Biophysical Differences between Human and Rat Members of ERG2 and ERG3. We have studied the steady-state voltage-dependent activation/inactivation and the time constants of activation in the six isoforms. Figure 1A shows that the activation curves of the human and rat ERG1 and

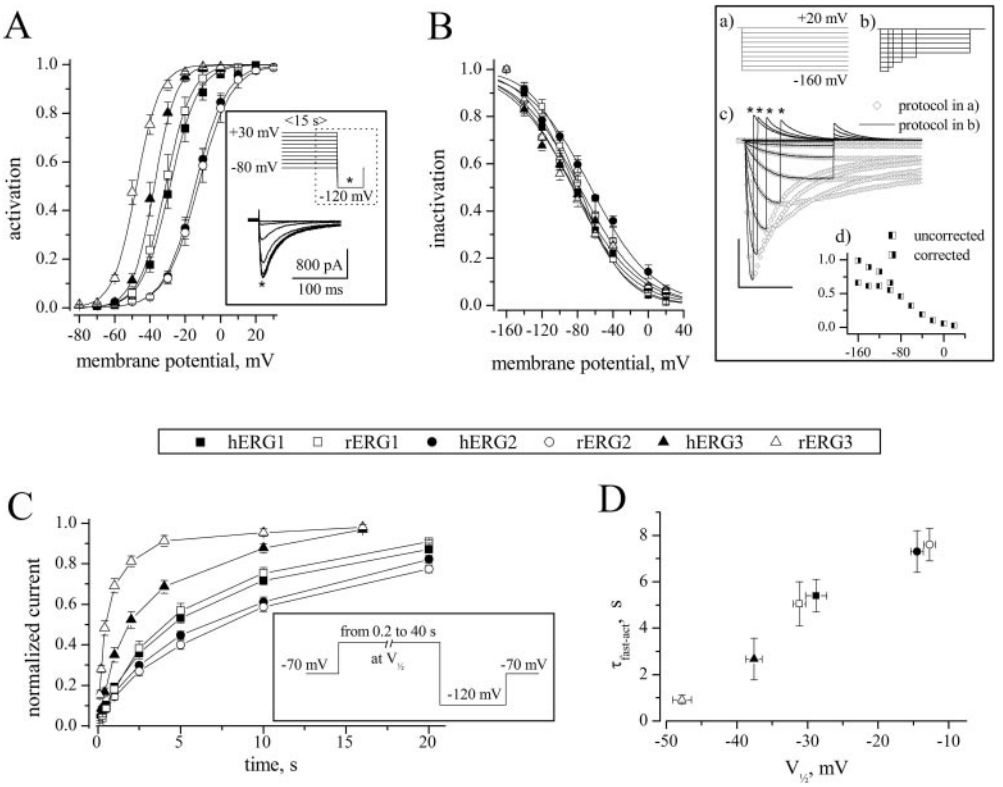

Fig. 1. Steady-state voltage-dependent activation and inactivation of ERG1, ERG2, and ERG3 human and rat channels. A, steady-state activation curves obtained from normalized peak currents elicited at −120 mV, after preconditioning for 15 s at potentials ranging from −80 to +30 mV (see inset for the protocol and a sample recording from hERG1). $V_{1/2}$ and slopes (millivolts) of 1, 2, and 3 isoforms were, respectively: for human, −28.7 ± 0.85, 7.9 ± 0.28; −14.5 ± 0.9, 8.77 ± 0.47; −37.6 ± 1.2, 6.12 ± 0.5; and for rat, −29.15 ± 1.52, 8.3 ± 0.4; −12.72 ± 0.85, 9.2 ± 0.4; −47.8 ± 1.3, 6.6 ± 0.5 (n = 8 for each member; see symbols in the central inset). B, steady-state inactivation curves from normalized extrapolated peak currents obtained as shown in the right inset (see *Materials and Methods* for details). $V_{1/2}$ and slopes (millivolts) of 1, 2, and 3 isoforms were, respectively: for human, −81.5 ± 1.8, 27.4 ± 1.7; −78.5 ± 1, 26.7 ± 1; −65.8 ± 2.1, 36.2 ± 2.0; for rat, −76.5 ± 2.2, 35.8 ± 3.1; −85.2 ± 3.1, 36.2 ± 3.0; −86.6 ± 4.1, 31.7 ± 2.1 (n = 6 for each members; same symbols as in A). Right inset, in a and b are shown the protocols used, in sequence, in the same cell, to obtain both the complete deactivation time course and the tail current at +20 mV. c, superimposed hERG1 currents elicited with the protocols in a and b. Data were corrected for deactivation at the negative voltage levels indicated by the asterisks (see *Materials and Methods*). Scale is 30 ms and 3 nA for x- and y-axis, respectively. d, tail currents from the cell in c are plotted before and after correction (left black square and right black square, respectively). C, time course of activation obtained by normalizing tails current at −120 mV after preconditioning each cell at its half-activation potential ($V_{1/2}$), for different durations (see protocol in the inset). Same symbols as in A and B. D, the fast time constant ($\tau_{fast\text{-}act}$) of the activation time course shown in C, is plotted versus $V_{1/2}$ (n = 4). Time constants for the rERG3, hERG3, rERG1, hERG1, hERG2, and rERG2 channels were, respectively (s), 0.92 ± 0.09, 2.67 ± 0.3, 5.05 ± 0.4, 5.4 ± 0.6, 7.3 ± 0.9, and 7.4 ± 0.8 (same symbols as in C).

ERG2 are almost superimposable. On the contrary, the hERG3 activation curve was found to be shifted to the left with respect to ERG1 by approximately 7 mV compared with the 17 mV observed in rERG3. The relative positions on the membrane potential axis of the three rat members [see half-activation potential ($V_{1/2}$) and slope values in the figure legend] closely correspond to those described previously (Wimmers et al., 2002; Sturm et al., 2005), apart from a few millivolts of negative shift as a result of the use of 40 mM $[K]_o$ instead of the normal 5 mM. On the other hand, the voltage-dependent inactivation curves of the human ERG1, ERG2, and ERG3 were very similar to each other (Fig. 1B). For rERG3, in the region from −40 to +40 mV, a shift to the right has been reported (Schledermann et al., 2001; Sturm et al., 2005) with respect to rERG1 and rERG2. Our data, obtained with the use of a different method (see inset and *Materials and Methods*) in a much larger voltage range from −160 to +20 mV, did not evidence this effect.

The time course of activation (Fig. 1C) was investigated with the envelope of the tail currents (see protocol in the inset) obtained at the $V_{1/2}$ calculated from the experiments shown in Fig. 1A. The time course could be fitted by a double-exponential function (data not shown). The slower time constant resulted in values larger than 30 s. Because it was not possible to condition the membrane potential for times longer than 40 s (to reach steady state), we decided to consider only the faster time constant, $\tau_{\text{fast-act}}$ (see legend to Fig. 1). These were entirely correlated with the $V_{1/2}$ values, as shown in Fig. 1D. Only for ERG3 channels were the values of the human and rat $\tau_{\text{fast-act}}$ significantly different (by a factor of ~3).

Another important property that differentiates the three rat members is the deactivation time course, which has been described by slow and fast components and a variable ratio of the slow to total amplitudes (Wimmers et al., 2002). Because the results we obtained with the hERG2 and hERG3 were different from those described by Wimmers et al. (2001) in the rat, we have tested all the above clones under the conditions applied by Schwarz et al. (2001) (extracellular solutions with 140 $[K]_o$ and 75 nM $[Ca^{2+}]_o$). In this case, we found that the biophysical features of the rat clones agreed with those reported by Wimmers et al. (2001) and that the differences

TABLE 1

Sequence alignments of human and rat ERG S5-S6 region

The complete sequence is shown only for hERG1, whereas for hERG2 and hERG3, only the residues that are different with respect to hERG1 are shown. Between each group of adjacent member rows (2–3, 4–5, 6–7), only the species different amino acids are indicated with respect to the human homologue. In the first row (STRUC), the hypothesized structural regions are indicated (black background indicates the putative α-helix). In the hERG1 row, the toxins-sensitive (BeKm-1, ErgTx1) residues are in white letter while those with gray or black background are important only for BeKm-1 or both toxins respectively (Zhang et al., 2003). The last two rows indicate the units and the tens of hERG1 sequence number starting from 568 and ending at 644. GenBank accession numbers: hERG1, NP_000229; hERG2, NP_110406; hERG3, NP_150375; rERG1, NP_446401; rERG2: O54853; rERG3, O54852.

```
1STRUC S5-<-S5-P-linker-------------S5-P Linker-->-<----P-loop---->-<P-S6link->-<S6
2hERG1 WYAIGNMEQPHMDSRIGWLHNLGDQIGKPYNSSGLG-GPSIKDKYVTALYFTFSSLTSVGFGNVSPNTNSEKIFSICV
3rERG1 --------------H-------------------------------------------------------------
4hERG2 ------V-R-YLEHK----DS--V-L--R--G-DPAS---VQ-----------------------------V-----
5rERG2 -------------P---------A----Q-------------------------------------------------
6hERG3 ------V-R-YLTDK----DS--Q----R--D-DSSS-----------------------------------------
7rERG3 ----------------------T-------------------------------------------------------
8unit  8901234567890123456789012345678901-2345678901234567890123456789012345678901234-
9tens  --7---------8---------9---------0----------1---------2---------3---------4----
```

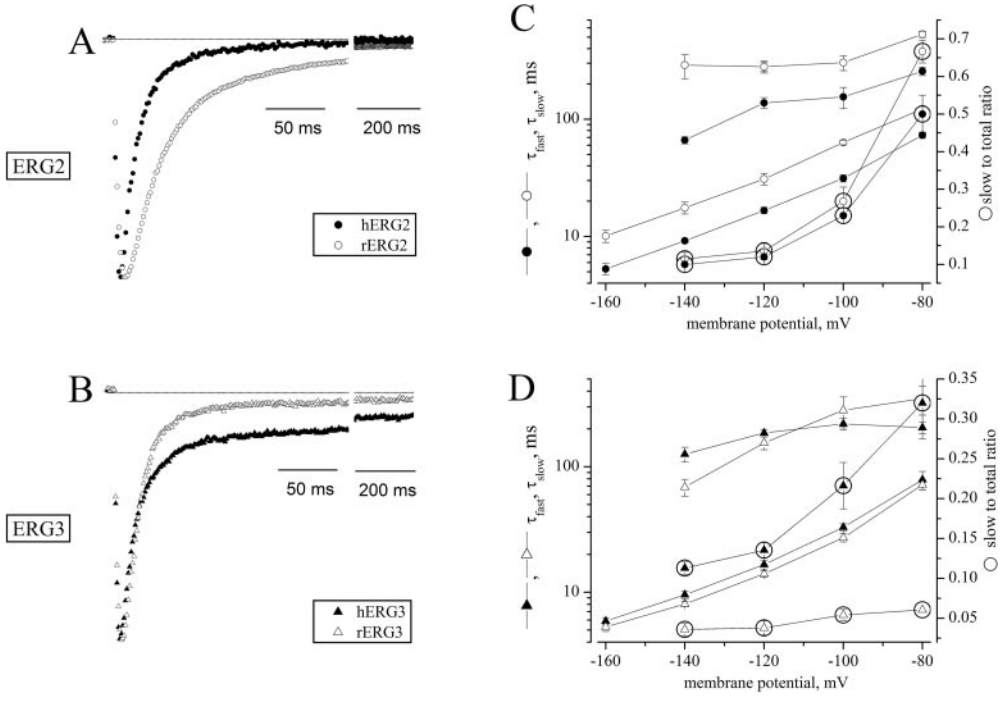

Fig. 2. Voltage-dependent deactivation kinetics of ERG2 (top) and ERG3 (bottom) observed in human and rat channels. A and B, superimposed ERG tail currents elicited at −120 mV (from 0 mV) for exemplary ERG2 and ERG3 expressing cells (symbols as indicated). Peak currents were normalized and trace lasted 1 s with a break from 0.2 to 0.8 s. C and D, plot of the deactivation time constants τ_{fast} and τ_{slow} at left *y*-axis as a function of the test potential, symbols as indicated, mean ± S.E.M. (n = 4 for each member). The ratio of slow component to total current is plotted with the right *y*-axis reference and symbols have been encircled to make clear that they refer to the right scale.

between rat and human ERG1 were not significant. On the contrary, the differences between the rat and human ERG2 and ERG3 persisted and thus are to be considered intrinsic properties of the channels (data not shown).

These differences were further investigated (Fig. 2). Normalized traces obtained from cells expressing ERG2 (Fig. 2A) and ERG3 (Fig. 2B) were superimposed, showing that hERG2 deactivates much faster than rERG2 at −120 mV. We ascribe the difference to the presence of a stretch of 36 amino acids in hERG2 but absent in rERG2; in fact, the C terminus has been demonstrated to be important for hERG1 deactivation kinetics (Aydar and Palmer, 2001). Moreover, hERG3 currents, although they decay similarly to rERG3, show a persistent component much larger than that of rERG3.

We measured, at negative membrane potential, the slow and fast time constants (Fig. 2, C and D, left *y*-axis) and the ratio of the slow to total current amplitudes (Fig. 2, C and D, right *y*-axis). Figure 2C shows that hERG2 (●) is characterized by τ_{fast} and τ_{slow} (at −120 mV, 16.7 ± 1.1 and 138 ± 15 ms, respectively) which are approximately half of those observed in rERG2 (○, 31 ± 3.5 and 280.85 ± 32.9 ms, respectively). The ratio of the slow to total current (encircled symbols) has an increasing voltage-dependent behavior that is not very different between rat and human (at −120 mV, 0.14 ± 0.02 and 0.12 ± 0.017, respectively). On the whole, these results account for the differences observed in A. Indeed, it has been reported (Wimmers et al., 2002) that in rERG2, the above ratio is almost 2-fold compared with rERG3, whereas rERG1 is in between.

On the contrary, as shown in Fig. 2D, hERG3 (▲) and rERG3 (△) have very similar values of τ_{fast} (at −120 mV, 16.6 ± 1.2 and 13.99 ± 0.74 ms, respectively) and τ_{slow} (at −120 mV, 186.1 ± 12.4 ms and 154.8 ± 17.9 ms, respectively), but the ratio of slow to total component amplitudes is from 3- to 5-fold higher in the human clone (at −120 mV, 0.14 ± 0.01 and 0.04 ± 0.01, respectively). Here again, the analysis substantiates the observations of B.

On the whole, these data suggest species-specific biophysical properties in ERG2 and ERG3 isoforms. For ERG2 channels, the difference consisted of a 2-fold faster deactivation of the human (●) isoform compared with the rat (○). For ERG3, species-related differences were present both in the steady-state activation (Fig. 1) and in the deactivation kinetics (Fig. 2D). In the former, we observed less negative $V_{1/2}$ values and slower activation in the human clone. In the deactivation kinetics, we found a 3- to 4-fold higher ratio of the slow to total component in hERG3 compared with rERG3. In principle, this diversity could help toxin peptides to discriminate the different channel proteins.

Non–Steady-State Properties of Toxin Blockade and Related Dose-Response Relationships. To test the speed, the amount of block, and the reversibility of action, we continuously perfused and voltage-clamped each cell (Fig. 3) at a fixed toxin concentration, with a protocol consisting of a test pulse at −120 mV delivered every 4 or 10 s and elicited either from an holding potential of −70 or +30 mV (Fig. 3, inset). This experimental protocol was necessary because our peptides have a voltage-dependent action, characterized by a loss of inhibition when the cell is depolarized (Gurrola et al., 1999). The toxin concentrations were chosen according to preliminary experiments to obtain significant inhibition. On the other hand, the dose-response curves were obtained by applying a large range of increasing toxin concentrations [T] (two values for each 10-fold [T] change), for 100 s. The effects were tested at −120 mV, from holding potentials of −70 mV. During these experiments, we could not check whether a steady-state condition was attained at the specific toxin concentration (because of the slowness of the effect). Therefore, some of the dose-response data might be affected by system-

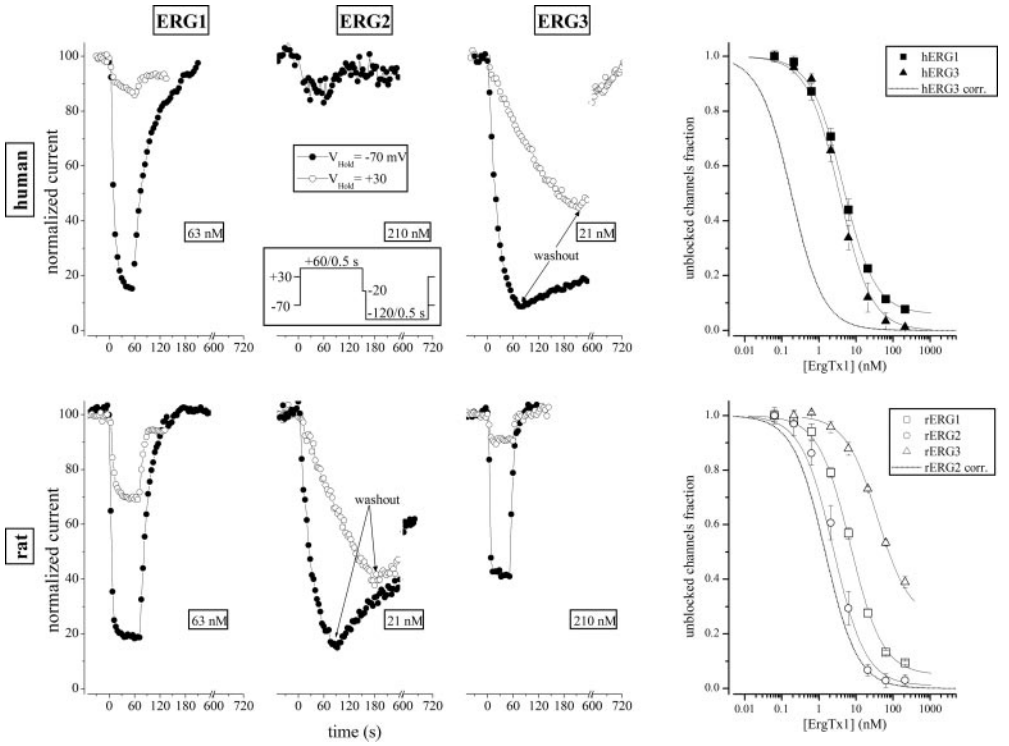

Fig. 3. ErgTx1-induced voltage-dependent blockade. Time plots of normalized I_{ERG} elicited by a 0.25 Hz pulse. Experiments were repeated from holding potentials of −70 mV (closed symbols) and +30 mV (open symbols) as indicated. Different concentrations were used to distinguish the voltage-dependent block. Note the break in the time axis. The two right plots are dose-response curves from experiments where negative holding potentials were used. Data were fitted to a logistic equation (power fixed to 1, line) where maximal fractional unblock, K_D (nanomolar) and number of experiments are shown in Table 3. The short dot sigmoidal line is the theoretical curve resulting from the K_D found during on-kinetics experiments; see text.

atic errors (i.e., underestimation of block), especially at the lowest concentrations, in which the "on kinetics" time constant was longer than 100 s. In these cases, the action of single toxin and the putative competition between some of the toxins were studied with different methods (see below).

TABLE 2

Block time and washout time constants of ErgTx1-induced blockade at different holding potentials for the human and rat ERG members (see Fig. 3)

Numbers of experiments were 3 and 2 for V_h equal to −70 or + 30 mV, respectively.

	Block Time (10–90%)		Washout Time Constant	
	V_h, −70 mV	V_h, +30 mV	V_h, −70 mV	V_h, +30 mV
	s			
Human				
ERG1	12.3 ± 3.6	N.A.	39.5 ± 1.8	N.A.
ERG2	N.A.	N.A.	N.A.	N.A.
ERG3	21 ± 3.3	N.A.	N.A.	302 ± 25
Rat				
ERG1	5.7 ± 3.2	6.2 ± 2.6	26.4 ± 3.4	N.A.
ERG2	48.3 ± 4.2	N.A.	430 ± 62	N.A.
ERG3	3.5 ± 0.7	N.A.	11.9 ± 4.2	N.A.

N.A., not analyzed.

TABLE 3

Dose-response curves properties for ErgTx1-induced blockade at −70 mV (see Fig. 3, right)

Ins is the fractional amount of toxin-insensitive ERG current, *N* is the number of experiments (K_D values in parenthesis derive from on-kinetics experiments).

	Ins	K_D	*N*
		nM	
Human			
ERG1	0.06	4.5 ± 0.3	5
ERG2	1	N.A.	3
ERG3	0	4.05 ± 0.32 (0.18 ± 0.03)	4
Rat			
ERG1	0.08	6.8 ± 0.21	5
ERG2	0.01	2.8 ± 0.19 (1.16 ± 0.09)	6
ERG3	0.25	38.1 ± 4.1	4

Properties of ErgTx1 Blockade. As shown in Fig. 3, the blockade rise time, the washout time constant, and the maximal block were different for the six channel types. The data for human and rat ERG1 substantially recapitulate (Gurrola et al., 1999) the fast action, the reversibility, and the voltage-dependent efficacy of this toxin (closed and open symbols are related to hyperpolarized or depolarized holding potentials). ErgTx1, up to 210 nM, was unable to consistently block hERG2 channels. On the contrary, full blockade of rERG2 was obtained around 21 nM at a relatively slow rate but with a poor reversibility because of a very slow unbinding kinetics. This effect was also observed on hERG3, but not on rERG3, where a weak blocking and washing-out was also obtained at 210 nM, during a 30-s application. In all clones, we observed a marked loss of potency at depolarized V_m (open symbols). The kinetics of block and recovery are summarized in Table 2.

A comparison of the quasi-stationary dose-response curves of the unblocked channel fraction (UCF; obtained from experiments in which negative holding potentials were used) is shown in the right of Fig. 3. Table 3 gives the parameters of the classic logistic equation with Hill coefficient fixed to 1, fitting the experimental data [we observed that a free Hill coefficient, between 0.98 to 1.26, could improve the fitting (data not shown)]. Table 3 also shows the fraction of current that is insensitive to high toxin concentrations (Ins). ErgTx1 blocked human ERG1 and ERG3 channels with a K_D of approximately 4 nM. On the contrary, the rat members were blocked with K_D ranging from 2.8 (ERG2) to 38 nM (ERG3).

On the whole, ErgTx1 had a greater affinity for rERG2 than for rERG1. Therefore, ErgTx1 represents the first high-affinity blocker for rERG2 channels, with a selectivity for rat over human members.

Properties of BeKm-1 Blockade. Experiments similar to those described for ErgTx1 were carried out for the other scorpion peptide BeKm-1, as reported in Fig. 4. Data show results obtained by applying 300 nM BeKm-1. In contrast to

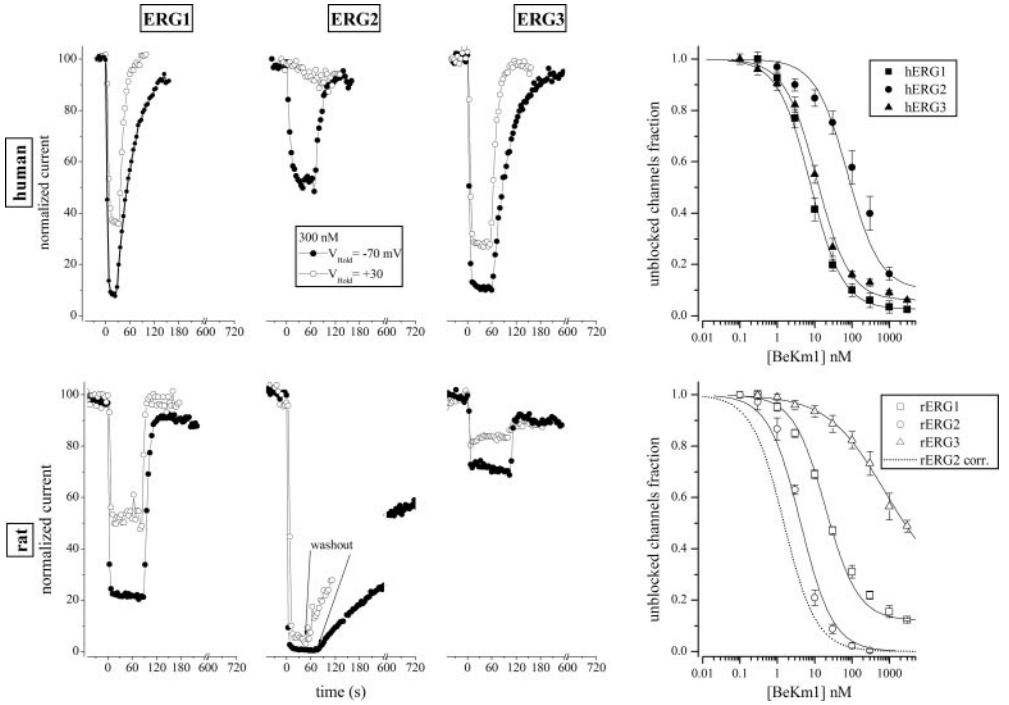

Fig. 4. BeKm-1-induced voltage-dependent blockade. Time plots of normalized I_{ERG} elicited by a 0.25-Hz pulse during perfusion of toxin at 300 nM. Experiments were repeated from holding potentials of −70 mV (closed symbols) and +30 mV (open symbols) as indicated. Notice the break in the time axis. The two right plots are dose-response curves from experiments where negative holding potentials were used. Data were fitted to a logistic equation (power fixed to 1, line) where maximal fractional unblock, K_D (nanomolar) and number of experiments are shown in Table 5. Data of rERG3 were fitted with a normal logistic at power 0.5. The short dot sigmoidal line is the theoretical curve resulting from the K_D found during on-kinetics experiments; see text.

ErgTx1, BeKm-1 was able to block all the six members, when applied at negative holding potential. Only hERG2 was insensitive to the toxin when the latter was applied at depolarized membrane potential. On washout, the recovery was always relatively fast, except for rERG2, recovery for which was extremely slow. Blocking and washout kinetic properties are summarized in Table 4.

The quasi-stationary dose-response curves (Fig. 4, far right, and Table 5) show an interesting pattern among the rat members, with different K_D values in the range from 4.2 to 747 nM. hERG1 and hERG3 were not discriminated by BeKm-1. On the contrary, it should be stressed that BeKm-1 was unique among the three toxins in its ability to block hERG2. Interestingly the rat members were sensitive to BeKm-1 with very different K_D values. Therefore, this toxin seems the most promising for selectively recognizing the functional roles of the three different clones.

Properties of APETx1 Blockade. The blocking properties of APETx1 are shown in Fig. 5, A and B. Because the peptide action is highly voltage-dependent (Diochot et al., 2003), experiments were performed at a very low pulse rate to rule out the toxin unbinding caused by the test pulse itself. APETx1 was unable to affect ERG2 and ERG3 currents at concentrations that saturated ERG1 (1 μM) and can therefore be considered a pure ERG1 blocker for both rat and human homologs.

Competition experiments between APETx1 (500 nM) and ErgTx1 (10 nM) or BeKm-1 (10 nM) have been performed, and results are shown in Fig. 5, C and D (human) and E and F (rat). The three columns of each graph show the fraction of unblocked channels under APETx1 alone, the competing toxin alone (ErgTx1 or BeKm-1), or both the competing toxins. These data should be compared with a hypothetical noncompetitive model, shown in Table 6. These results are consistent with the notion that the binding sites on ERG1 for APETx1 are far apart from those of ErgTx1 and BeKm-1 (Diochot et al., 2003; Chagot et al., 2005).

On Kinetics and Competition Experiments with BeKm-1 and ErgTx1. The data shown in Figs. 3 and 4 were obtained with different concentrations of ErgTx1 and BeKm-1. Nonetheless, they suggest important differences between these toxins, if we compare the time constants of washout, which should depend only on the dissociation rates and not on the toxin concentration. Both toxins showed a very fast dissociation from rERG3, whereas the longest time constants for washout were observed for hERG3 and rERG2. The similarities between the two toxins suggest that competition for similar regions of these channels might influence the on kinetics when both toxins are present. Because overlapping binding sites on hERG1 have been suggested for ErgTx1 and BeKm-1 (Zhang et al., 2003), we have also studied their competition for hERG3 and rERG2. These experiments allowed us to calculate the K_D of these effects with much more precision than was possible from the data given in Tables 3 and 5.

As for BeKm-1 and its dose-response curves (Fig. 4), we can estimate whether the 100 s used to equilibrate toxin binding, was sufficient to reach the steady-state, based on the expected time constant τ_{on} measured during an on-kinetics experiment and theoretically predicted by eq. 4 (see *Materials and Methods*). The K_D values for hERG1 and hERG3 derived from fitting were approximately 9 nM (see Table 5) and the τ_{off} were approximately 50 s (see Table 4). Thus, at 3 nM, the calculated τ_{on} is approximately 38 s; i.e., a 115-s delay should occur to approximate the steady-state condition for the dose-response curve.

For rERG2, the K_D for BeKm-1, derived from the dose-response curve, was 4.2 nM and the washout time constant was around 300 s, leading to a τ_{on} (at 3 nM) of 175 s and to an experimental time of approximately 9 min. In this case, a specific kinetic experiment is essential to clarify and calculate the correct K_D using either eq. 1 or eq. 5.

Competition experiments should be done at concentrations close to the respective K_D values to determine whether the results depend on pure summation of the effects or competition. This is particularly difficult, however, from an experimental point of view, because at these concentrations, the on kinetics are very slow.

Competition on hERG3 Channels. Data from Table 5 suggest a putative BeKm-1 K_D of 11.5 nM, and we thus studied the kinetics of inhibition at 20 nM. From the average of four experiments, shown in Fig. 6A, we obtained a mean UCF of 0.41 ± 0.03 and τ_{on} = 22.8 ± 2.9 s (Fig. 6, D and E, first bars). By using this UCF value in eq. 1, we found $K_D = 20 \times (1/0.41 - 1)^{-1} = 13.9$ nM, and, by using the τ_{on} and τ_{off} values in eq. 2, we found $K_D = 20 \times 22.8/(58 - 22.8) = 13$ nM.

These values are in good agreement with the value of 11.5 nM shown in Table 5. The same procedure was applied at 2 nM ErgTx1 (Fig. 6B, $n = 3$). In this case, τ_{on} was 34.1 ± 4.5 s and UCF was 0.08 ± 0.02 (Fig. 6, D and E, third bar). Because τ_{off} was very poorly defined, we did not use eq. 2.

TABLE 4

Block time and washout time constants of BeKm-1-induced blockade at different holding potentials for the human and rat ERG members (see Fig. 4)

Numbers of experiments were 3 and 2 for V_h equal to −70 or + 30 mV, respectively.

	Block Time (10–90%)		Washout Time Constant	
	V_h, −70 mV	V_h, +30 mV	V_h, −70 mV	V_h, +30 mV
	s			
Human				
ERG1	7 ± 0.5	8.8 ± 1	42 ± 1.1	14 ± 0.76
ERG2	32 ± 2.5	N.A.	15 ± 0.67	N.A.
ERG3	7 ± 0.9	11 ± 1.8	57.7 ± 3.2	13.3 ± 1.1
Rat				
ERG1	3.1 ± 1	2.9 ± 1	5 ± 0.4	12 ± 1.1
ERG2	3.3 ± 1	5 ± 1.3	313 ± 18	208 ± 13
ERG3	2.5 ± 0.7	2.3 ± 0.6	2.3 ± 0.13	N.A.

N.A., not analyzed.

TABLE 5

Dose-response curves properties for BeKm-1-induced blockade at −70 mV (see Fig. 4, right)

Ins is the fractional amount of toxin-insensitive ERG current, *N* is the number of experiments (K_D values in parenthesis derive from on-kinetics experiments).

	Ins	K_D	*N*
		nM	
Human			
ERG1			
ERG2	0.025	7.7 ± 0.6	8
ERG3	0.1	77 ± 16	5
Rat	0.06	11.5 ± 1.1	6
ERG1	0.12	19 ± 1.6	6
ERG2	0	4.2 ± 0.5 (1.51 ± 0.12)	5
ERG3	0.25	747 ± 58	6

From eq. 1, as before, we found $K_D = 2 \times (1/0.08 - 1)^{-1} = 0.18$ nM, which is approximately 20 times smaller than the value derived from the dose-response curves of Fig. 3 (see also Table 3). The dose-response theoretical curve with this K_D is shown in short points in Fig. 3, top right .

With the mixture of toxins (BeKm-1was applied first), we tested five cells. One experiment is shown in Fig. 6C, where the block produced by the competing toxins reached 0.11 ± 0.02 and the τ_{on} of the current decay was 274 ± 35 s (Fig. 6, D and E, second bar). Both values are in disagreement with a model of independent action because, in this case, we would expect (1) a block down to 0.033, which is approximately 3-fold smaller than the experimental value, and (2) a τ_{on} equal to 34.1 s (the line in the plot of Fig. 6C), which is approximately eight times smaller than the experimental result. We were unable to apply the toxins in reverse order, because we should have used a much smaller ErgTx1 concentration, with an impractical increase in the total experimental time, because of current run-down. Overall, these findings suggest a net competition between the two toxins.

Affinity and Competition on rERG2 Channels. Before performing a competition experiment, we wanted a better estimate the K_D values of both ErgTx1 and BeKm-1 for comparison with the approximate values of 2.8 and 4.2 nM derived in Figs. 3 and 4.

To this aim, we used eq. 5 at two different pairs of $[T_1]$ and $[T_2]$ concentrations, either 2 nM and 10 nM or 2 nM and 20 nM. The results were averaged to obtain a more precise value. These τ_{on} were measured as shown in Fig. 7, A and B, for the pair of concentrations 2 and 10 nM. At 2 nM, τ_{on} resulted 134.3 ± 6.2 ($n = 5$) for BeKm-1 (□) and 140.2 ± 6.7 ($n = 6$) for ErgTx1 (○). At 10 nM, τ_{on} were 38.2 ± 0.8 ($n = 4$) for BeKm-1 (■) and 31.6 ± 0.7 s ($n = 7$) for ErgTx1 (●). The corresponding values at 20 nM were 20 ± 1.2 s for BeKm-1and 23 ± 1.3 s for ErgTx1 ($n = 4$). These values are plotted as bars in Fig. 7E. In addition, we measured the UCF at 2 nM, which was 0.18 ± 0.02 for BeKm-1 and 0.13 ± 0.15 for ErgTx1.

By inserting the above data in eq. 5, we calculated the K_D values, that turned out to be 1.51 ± 0.12 for ErgTx1 and 1.16 ± 0.09 for BeKm-1. These values were quite different from those shown in Figs. 3 and 4 (see also Tables 4 and 5). Because the latter were obtained at the steady state, their accuracy is expected to be higher. The dose-response theoretical curves with the corresponding K_D values are shown in short points in Figs. 3 and 4, far right.

For competition experiments, we decided to use the 2 and 10 nM concentrations as the first and the second applications, respectively. To verify whether competition took place at the moment of the second application, only the time constant of the second application was analyzed. We decided not to include in the analysis the amplitude (small) of the current blocked during the second toxin application, because in each experiment we usually detected a variable amount (3–6%) of unblocked current, which could be a further source of error.

If competition is effective, we would measure a τ_{on} significantly longer than the one observed in single toxin experiment. Two exemplary competition experiments (of 11 total) are shown in Fig. 7C (BeKm-1 applied first) and in Fig. 7D (opposite order). Although the observed τ_{on} fluctuated con-

TABLE 6

UCF resulting during competition experiments between APETx1 and ErgTx1 or BeKm-1 (number of experiments is in parenthesis)

The theoretically expected values under no competition are shown. Values are presented as mean± S.E.M.

	Human	Rat
APETx1	0.81 ± 0.03 (9)	0.81 ± 0.04 (4)
BeKm-1	0.54 ± 0.04 (10)	0.66 ± 0.02 (4)
Both	0.40 ± 0.02 (13)	0.50 ± 0.04 (5)
Theoretical	0.43 ± 0.04	0.53 ± 0.05
APETx1	0.68 ± 0.06 (6)	0.82 ± 0.06 (4)
ErgTx1	0.37 ± 0.02 (9)	0.50 ± 0.03 (6)
Both	0.21 ± 0.03 (4)	0.32 ± 0.03 (3)
Theoretical	0.25 ± 0.07	0.41 ± 0.06

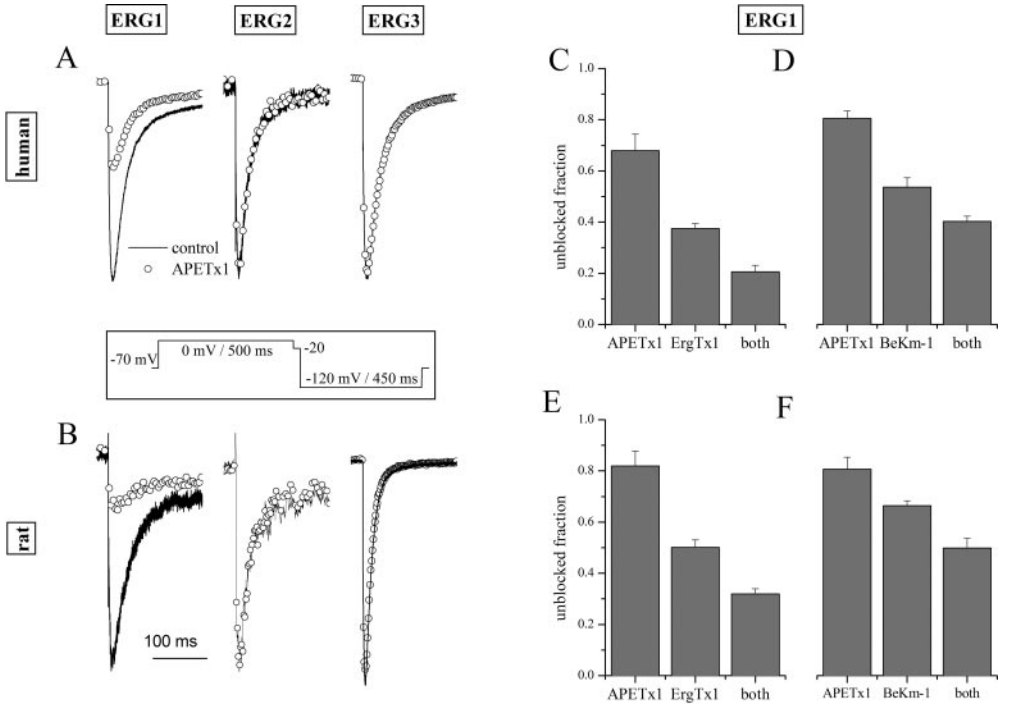

Fig. 5. The properties of the APETx-1 peptide. A and B, in the six are shown the superimposed traces of ERG currents elicited with the protocol shown in the inset. Human and rat ERG1, ERG2, and ERG3 currents are shown in the upper and lower in control conditions (lines) and during APETx1 perfusion. Concentrations were on hERG1 at 0.5 μM; on rERG1 at 1 μM; on ERG2 and ERG3 at 2 μM. C and D, summary of the results of competition experiments performed with APETx1 (500 nM, left bars) or ErgTx1 (10 nM, middle bar) and with both toxins applied in the two different orders. Number of experiments (APETx1, ErgTx1, both) were for hERG1 and rERG1 5, 4, 8 and 4, 3, 6.

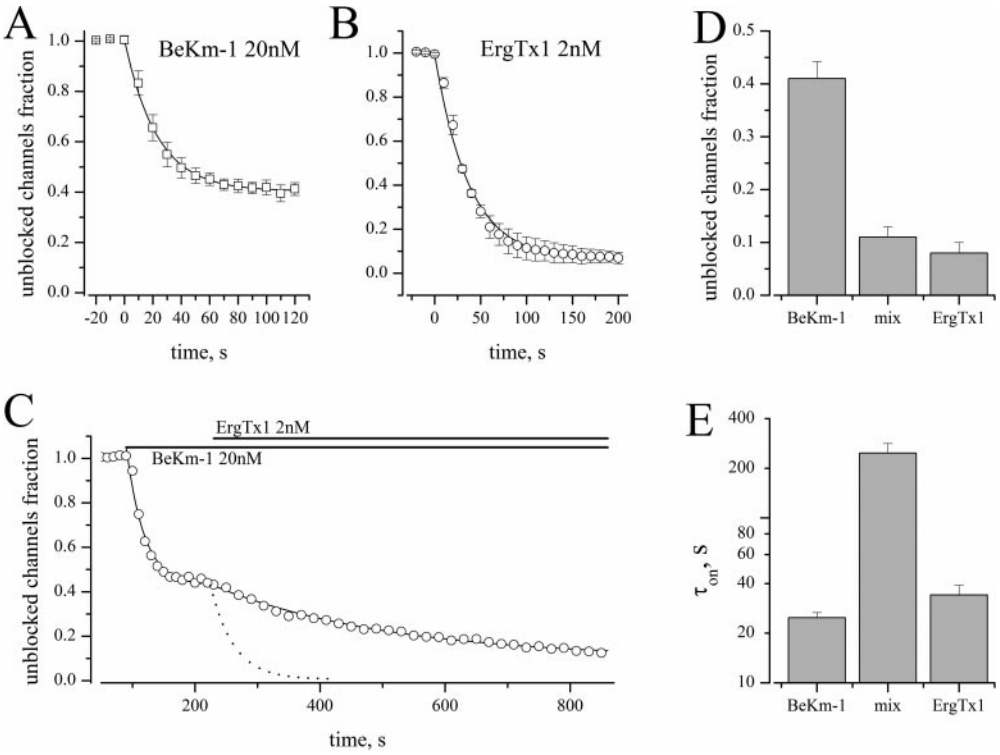

Fig. 6. Competition experiments on hERG3 between ErgTx1 and BeKm-1. A, time course of the mean± S.E.M. of four kinetic experiments during perfusion of 20 nM BeKm-1 (□), starting at time 0. Test pulses every 10 s. The line is the best fit to an exponential decay with time constant of 22.8 ± 2.9 s. B, same as A but 2 nM ErgTx1 (○) and $n = 3$. The line is the best fit to an exponential decay with time constant of 34.1 ± 2.4 s. C, one of the five competition experiments in which BeKm-1 (○, 20 nM) was applied first and then ErgTx1 (2 nM) at the indicated instants. The first continuous line during BeKm-1 was the best fit to an exponential decay with a time constant of 29.2 ± 3.3 s and the second line was the best fit to an exponential decay with a time constant of 285.5 ± 13.4 s. The dashed line starting at the beginning of the mixture perfusion is the predicted time course under the hypothesis of no competition (same exponential as that shown in B). D, plot of the τ_{on} during on-kinetics single or combined experiments with 20 nM BeKm-1 ($n = 4$), 2 nM ErgTx1 ($n = 3$), or a mixture of both ($n = 5$). E, same as in D but plot of the unblocked channels fraction.

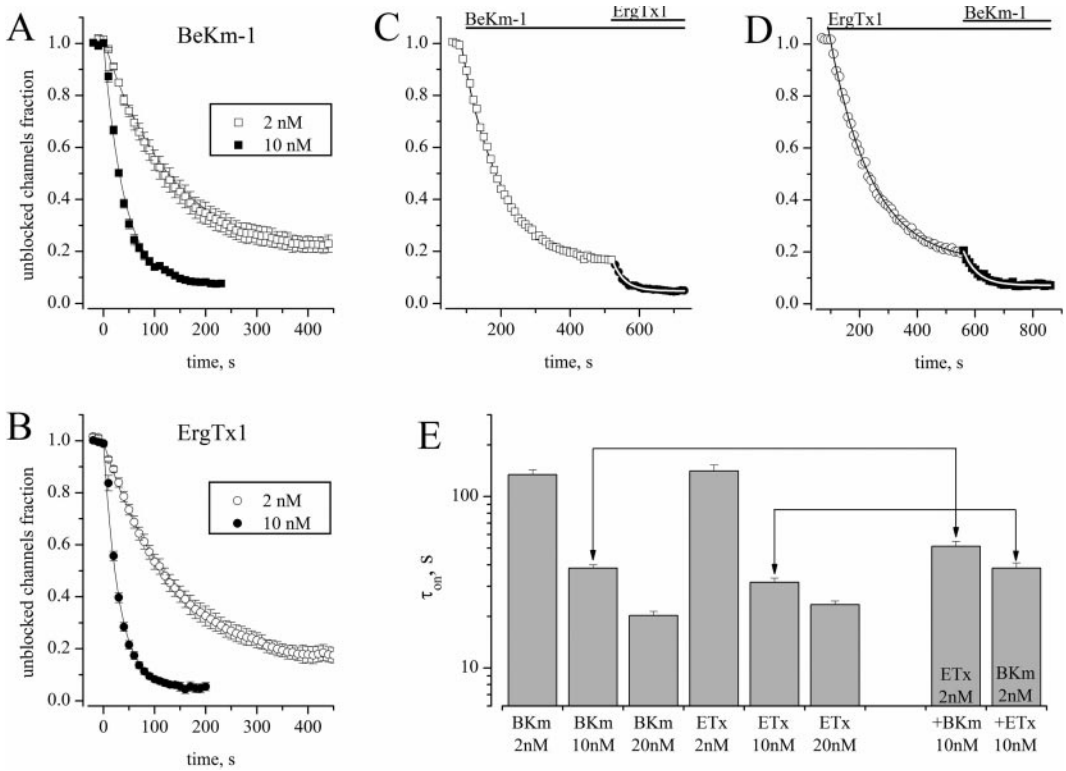

Fig. 7. Competition experiments on rERG2 between ErgTx1 and BeKm-1. A, time course of on-kinetic experiments (mean ± S.E.M.; start at time 0) at 2 (□) and 10 (■) nM BeKm-1. Test pulses every 10 s. The lines are the best fit to exponential decays with time constants of 134.3 ± 6.2 ($n = 5$) and 38.2 ± 0.8 ($n = 4$). B, same as A but ErgTx1 was used (○, 2 nM; ●, 10 nM). The line is the best fit to an exponential decay with time constant of 140.2 ± 6.7 ($n = 6$) and 31.6 ± 0.7 ($n = 7$). C and D, two of the 11 competition experiments in which BeKm-1 (□, 2 nM) or ErgTx1 (○, 2 nM) were applied first at the indicated instants and then the other toxin as indicated. The continuous black lines were the best fit to an exponential decay with time constant of 117.9 ± 7.8 s (for BeKm-1) and 145.6 ± 8.7 s (for ErgTx1). The second white lines through the black symbols were the best fit to an exponential decay with a time constants of 34.1 ± 1.4 s (for BeKm-1) and 49.2 ± 2.6 s (for ErgTx1). E, plot of the τ_{on} during on-kinetics, single or combined experiments, at the indicated toxin concentrations. The τ_{on} of the second application were 51.2 ± 3.5 s when BeKm-1 was the second and 38.2 ± 2.9 s when ErgTx1 was the second. Number of experiments with 2 nM BeKm-1 first was six and those with 2 nM ErgTx1 first were five.

siderably among experiments, the relatively fast time course of current decay (white lines through symbols) were little different from the mean values of the corresponding time constants measured during single toxin applications. Averaged data are shown in Fig. 7E, and the experiments to be compared are highlighted by the arrows. In conclusion, it seems that the binding of one toxin is not affected to a greater extent by the presence of the other toxin because the respective time constants were only increased marginally (from 38.2 ± 0.8 s to 51.2 ± 3.5 s for BeKm-1 and from 31.6 ± 0.7 s to 38.2 ± 2.9 s for ErgTx1). Therefore, the two toxins did not compete for the same binding site on rERG2.

Discussion

In general, biophysical properties are the hallmark of voltage-dependent ion channels, but gene subfamilies are often composed of clones with very similar properties. Because subfamilies have subtle differences and are often characterized by unique tissue-specific and sometimes species-specific distributions, the use of highly selective drugs or peptides able to distinguish basically similar biophysical behavior is urgently needed (Wimmers et al., 2001, 2002). In the present study, we showed, for the first time, that some voltage-dependent ERG K^+ channels, almost indistinguishable from a biophysical standpoint, could be isolated by using appropriate concentration of pure peptides.

As shown before by Shi et al. (1997), the amino acid identities among hERG1 and rERG2 or rERG3 is around 60 ± 3%. On the contrary, we found that the similarity between the same isoform in two species (human and rat) turned out to be very high: 95% for ERG1, 90% for ERG2, and 94% for ERG3.

Although ERG1, ERG2, and ERG3 are very similar in their primary sequences and biophysical properties, we showed that three ERG1-specific toxins, APETx1, BeKm-1, and ErgTx1, with no sequence homology, can distinguish both the rat and human members, with K_D values ranging from 0.18 to 747 nM.

Moreover, we found that the biophysical properties of ERG2 and ERG3, compared across humans and rats, are substantially different. Although there is still no evidence of the regional distribution of hERG2 and hERG3 channels in the human CNS, these biophysical differences suggest that hERG2 and hERG3 exert different functional roles, with possible consequences on the neuronal excitability in specific CNS areas.

Concerning the blocking properties studied here, we observed that the potency rank order for ErgTx1 suggests the following sequence (in parentheses are nanomolar K_D values):

hERG3 (0.18) ≫ hERG1 (4.5)
rERG2 (1.16) > rERG1 (6.8) > rERG3 (38)

whereas for BeKm-1, the K_D values rank as follows:

hERG1 (7.7) > hERG3 (11.5) ≫ hERG2 (77)
rERG2 (1.51) ≫ rERG1 (19) ≫ rERG3 (747).

As for the species differences, we observed that the sea anemone APETx1 was not able to recognize the less primordial channels ERG2 and ERG3. On the contrary, the ratio of the rat and human K_D values for each member ($^{ErgTx1}K_{Dr/h}$ (x) and $^{BeKm-1}K_{Dr/h}$ (x), x = 1,2,3) suggests that there is a consistency between the two scorpion toxins' preference. Indeed, in the case of ErgTx1, hERG1 and hERG3 are better recognized than the rat members ($K_{Dr/h}$(ERG1) = 1.5, $K_{Dr/h}$(ERG3) = 211), whereas the opposite is true for ERG2, a human clone not recognized by ErgTx1. For BeKm-1, the situation is similar because both $K_{Dr/h}$(ERG1) = 2.7 and $K_{Dr/h}$(ERG3) = 65 are much higher than 1, and $K_{Dr/h}$(ERG2) = 0.02 is much less than 1.

It is known that the S5-P linker of the hERG1 channel is important for high-affinity binding of ErgTx1 and BeKm-1 (Pardo-López et al., 2002; Zhang et al., 2003). Natural amino acid substitutions in this region of ERG2 and ERG3 proteins considerably change toxin affinity. One rERG3 mutation compared with hERG3 (Q591T) results in decrease of BeKm-1 affinity by ~65-fold, and triple mutation in hERG2 compared with rERG2 makes this channel insensitive to ErgTx1 (P581H, A591V, and Q596R). On the other hand, BeKm-1 and ErgTx1 most likely share a similar mechanism of action, suggesting similarities in their interaction surfaces and overlapping binding sites, at least on ERG1 and ERG3. On the contrary, APETx1 must have a different target region on ERG1. Results shown in the present paper should be helpful for modeling of toxin interaction and to study the structure of outer vestibules of ERG channels.

In addition, our data are relevant for designing experiments aimed at determining the physiological roles of different clones. Moreover, it could be of particular interest in humans, because it cannot be excluded that epilepsy episodes could depend on disorders originating from mutant ERG channels.

The ideal drug should have K_D values (with a Hill coefficient around 1) that differ at least 6-fold among different channels. In this case, at a concentration of $6 \times K_D$, only 16% of the channels with the lowest K_D will remain open compared with 84% of the channels with the higher K_D. To design blocking experiments in rat (and almost certainly in mouse), the best case would be to start with rERG2, because BeKm-1 toxin presents the advantage of having the largest K_D difference among the three channels in rat. By using BeKm-1 (at 9 nM) first, it is possible to obtain a 84% rERG2 blockade. This procedure should also produce a small effect on rERG1 (32%). Further application of BeKm-1 (at 114 nM) should almost completely block rERG1; BeKm-1 at very high concentration or ErgTx1 (at 228 nM) should inhibit rERG3. On the contrary, if rERG1 blockage is to be achieved first, APETx1 should be used, followed by either ErgTx1 (at 7 nM) or BeKm-1 (at 9 nM) for rERG2 blockade, and finally ErgTx1 (at 228 nM) for blocking rERG3. Other types of procedures should be used if working on human tissues: first, use APETx1 to block hERG1, then at least 1.8 nM ErgTx1 for an almost complete blockade of hERG3, and finally BeKm-1, at 770 nM, for blocking hERG2.

We have not investigated in the present work the very interesting problems concerning the possibility that heteromultimeric channels could also coassemble in the CNS (Hirdes et al., 2005). It is possible that the K_D values for heteromultimers are different from those reported here. This type of study, which complicates the research, is in progress.

References

Akbarali HI, Thatte H, He XD, Giles WR, and Goyal RK (1999) Role of HERG-like K^+ currents in opossum esophageal circular smooth muscle. *Am J Physiol* **277:**C1284–C1290.

Aydar E and Palmer C (2001) Functional characterization of the C-terminus of the human *ether-à-go-go*-related gene K^+ channel. *J Physiol* **534:**1–14.
Chagot B, Diochot S, Pimentel C, Lazdunski M, and Darbon H (2005) Solution structure of APETx1 from the sea anemone *Anthopleura elegantissima*: a new fold for an HERG toxin. *Proteins* **59:**380–386.
Chiesa N, Rosati B, Arcangeli A, Olivotto M, and Wanke E (1997) A novel role for ERG K^+ channels: spike frequency adaptation. *J Physiol* **501:**313–318.
Corrette BJ, Bauer CK, and Schwarz JR (1996) An inactivating inward-rectifying K current present in prolactin cells from the pituitary of lactating rats. *J Membr Biol* **150:**185–195.
Diochot S, Loret E, Bruhn T, Beress L, and Lazdunski M (2003) APETx1, a new toxin from sea anemone *Anthopleura elegantissima*, blocks voltage-gated human *ether-à-go-go*-related potassium channels. *Mol Pharmacol* **64:**59–69.
Guasti L, Cilia E, Crociani O, Hofmann G, Polvani S, Becchetti A, Wanke E, Tempia F, and Arcangeli A (2005) Expression pattern of the *ether-à-go-go*-related (ERG) family proteins in the adult mouse central nervous system: evidence for coassembly of different subunits. *J Comp Neurol* **491:**157–174.
Gullo F, Ales E, Rosati B, Lecchi M, Masi A, Guasti L, Cano-Abad MF, Arcangeli A, Lopez MG, and Wanke E (2003) ERG K^+ channel blockade enhances firing and epinephrine secretion in rat chromaffin cells: the missing link to LQT2-related sudden death? *FASEB J* **17:**330–332.
Gurrola GB, Rosati B, Rocchetti M, Pimienta G, Zaza A, Arcangeli A, Olivotto M, Possani LD, and Wanke E (1999) A toxin to nervous, cardiac and endocrine ERG K^+ channels isolated from *Centruroides noxius* scorpion venom. *FASEB J* **13:**953–962.
Gutfreund H (1995) *Kinetics for the Life Sciences: Receptors, Transmitters and Catalysts.* Cambridge University Press, Cambridge.
Hirdes W, Schweizer M, Schuricht KS, Guddat SS, Wulfsen I, Bauer CK, and Schwarz JR (2005) Fast erg K^+ currents in rat embryonic serotonergic neurons. *J Physiol* **554:**33–49.
Korolkova YV, Kozlov S, Lipkin AV, Pluzhnikov KA, Hadley JK, Filippov AK, Brown DA, Angelo K, Strobaek D, Jespersen T, et al. (2001) An ERG channel inhibitor from the scorpion *Buthus eupeus. J Biol Chem* 276:9868–9876.
Lecchi M, Redaelli E, Rosati B, Gurrola G, Florio T, Crociani O, Curia G, Restano Cassulini R, Masi A, Arcangeli A, et al. (2002) Isolation of a long-lasting ERG-type K^+ current in MMQ lactotrophs and its accommodating role during slow firing and prolactin release. *J Neurosci* **22:**3414–3425.
Nastainczyk W, Meves H, and Watt DD (2002) A short-chain peptide toxin isolated from *Centruroides sculpturatus* scorpion venom inhibits *ether-à-go-go*-related gene K^+ channels. *Toxicon* **40:**1053–1058.
Oliveira JS, Redaelli E, Zaharenko AJ, Restano Cassulini R, Konno K, Pimenta DC, Freitas JC, Clare JJ, and Wanke E (2004) Binding specificity of sea anemone toxins to Na_v 1.1–1.6 sodium channels: unexpected contributions from differences in the IV/S3–S4 outer loop. *J Biol Chem* **279:**33323–33335.
Overholt JL, Ficker E, Yang T, Shams H, Bright GR, and Prabhakar NR (2000) HERG-like potassium current regulates the resting membrane potential in glomus cells of the rabbit carotid body. *J Neurophysiol* **83:**1150–1157.
Papa M, Boscia F, Canitano A, Castaldo P, Sellitti S, Annunziato L, and Taglialatela M (2003) Expression pattern of the *ether-à-gogo*-related (ERG) K^+ channel-encoding genes ERG1, ERG2, and ERG3 in the adult rat central nervous system. *J Comp Neurol* **466:**119–135.
Pardo-López L, Zhang M, Liu J, Jiang M, Possani LD, and Tseng GN (2002) Mapping the binding site of a human *ether-à-go-go*-related gene-specific peptide toxin (ErgTx) to the channel's outer vestibule. *J Biol Chem* **277:**16403–16411.
Polvani S, Masi A, Pillozzi S, Gragnani L, Crociani O, Olivotto M, Becchetti A, Wanke E, and Arcangeli A (2003) Developmentally regulated expression of the mouse homologues of the potassium channel encoding genes merg1, merg2, and merg3. *Gene Expr Pattern* **3:**767–776.
Rosati B, Marchetti P, Crociani O, Lecchi M, Lupi R, Arcangeli A, Olivotto M, and Wanke E (2000) Glucose- and arginine-induced insulin secretion by human pancreatic b-cells: the role of HERG K^+ channels in firing and release. *FASEB J* **14:**2601–2610.
Sacco T, Bruno A, Wanke E, and Tempia F (2003) Functional roles of an ERG current isolated in cerebellar Purkinje neurons. *J Neurophysiol* **90:**1817–1828.
Saganich MJ, Machado E, and Rudy B (2001) Differential expression of genes encoding subthreshold-operating voltage-gated K^+ channels in brain. *J Neurosci* **21:**4609–4624.
Sanguinetti MC, Jiang C, Curran ME, and Keating MT (1995) A mechanistic link between an inherited and acquired cardiac arrhythmia: HERG encodes the Ikr potassium channel. *Cell* **81:**299–307.
Sanguinetti MC and Jurkiewicz NK (1990) Two components of cardiac delayed rectifier K^+ current. *J Gen Physiol* **96:**195–215.
Schledermann W, Wulfsen I, Schwarz JR, and Bauer CK (2001) Modulation of rat erg1, erg2, erg3 and HERG K^+ currents by thyrotropin-releasing hormone in anterior pituitary cells via the native signal cascade. *J Physiol* **532 (Pt 1):**143–163.
Schönherr R, Rosati B, Hehl S, Rao VG, Arcangeli A, Olivotto M, Heinemann SH, and Wanke E (1999) Functional role of the slow activation property of ERG K^+ channels. *Eur J Neurosci* **11:**753–760.
Shi W, Wymore RS, Wang HS, Pan Z, Cohen IS, McKinnon D, and Dixon JE (1997) Identification of two nervous system-specific members of the *erg* potassium channel gene family. *J Neurosci* **17:**9423–9432.
Smith PL, Baukrowitz T, and Yellen G (1996) The inward rectification mechanism of the HERG cardiac potassium channel. *Nature (Lond)* **379:**833–836.
Spinelli W, Moubarak IF, Parson RW, and Colatsky TJ (1993) Cellular electrophysiology of WAY 123,398, a new class III antiarrhythmic agent: specificity and frequency-independence of Ik block in cat ventricular myocytes. *Cardiovasc Pharmacol* **93:**1580–1589.
Sturm P, Wimmers S, Schwarz JR, and Bauer CK (2005) Extracellular potassium effects are conserved within the rat ERG K^+ channel family. *J Physiol* **564:**329–345.
Torres AM, Bansal PS, Sunde M, Clerke CE, Bursill GA, Smith DJ, Bauskin A, Breit SN, Campbell TJ, Alewood PF, et al. (2003) Structure of the HERG K^+ channel S5P extracellular linker: role of an amphipathic alpha-helix in C-type inactivation. *J Biol Chem* **278:**42136–42148.
Titus SA, Warmke JW, and Ganetzky B (1997) The *Drosophila erg* K^+ channel polypeptide is encoded by the seizure locus. *J Neurosci* **17:**875–881.
Warmke JW and Ganetzky B (1994) A family of potassium channel genes related to *eag* in *Drosophila* and mammals. *Proc Natl Acad Sci USA* **91:**3438–3442.
Wimmers S, Wuflsen I, Bauer CK, and Schwarz JR (2001) Erg1, erg2 and erg3 K channel subunits are able to form heteromultimers. *Pflueg Arch Eur J Physiol* **441:**450–455.
Wimmers S, Bauer CK, and Schwarz JR (2002) Biophysical properties of heteromultimeric erg K^+ channels. *Pflueg Arch Eur J Physiol* **445:**423–430.
Zhang M, Korolkova YV, Liu J, Jiang M, Grishin EV, and Tseng GN (2003) BeKm-1 is a HERG-specific toxin that shares the structure with ChTx but the mechanism of action with ErgTx1. *Biophys J* **84:**3022–3036.

Address correspondence to: Prof. Enzo Wanke, Dipartimento di Biotecnologie e Bioscienze Università di Milano-Bicocca, Piazza della Scienza 2, 20126 Milano, Italy. E-mail: enzo.wanke@unimib.it